Supporting Information

Promoting C-C Coupling for CO_2 Reduction on Cu_2O Electrocatalysts with Atomically Dispersed Rh Atoms

1. Synthesis of materials

All chemicals are analytical grade and are used as purchased without further purification. The details are as follows: Copper (II) sulfate pentahydrate ($CuSO_4 \cdot 5H_2O$, 99.0%, Sinopharm Chemical Reagent Co., Ltd.), sodium rhodium chloride dodecahydrate ($Na_3RhCl_6 \cdot 12H_2O$, Rh 17.1%, Alfa Aesar), oleic acid ($C_{18}H_{34}O_2$, Sinopharm Chemical Reagent Co., Ltd.), ethanol (C_2H_5OH, 99.5%, Sinopharm Chemical Reagent Co., Ltd.), sodium hydroxide (NaOH, 96%, Sinopharm Chemical Reagent Co., Ltd.), D-(+)-glucose (Sinopharm Chemical Reagent Co., Ltd.), tetra-n-butylammonium hexafluorophosphate ($BminPF_6$, J&K Reagent Co., Ltd.), potassium hydrogen carbonate ($KHCO_3$, 99.5%, Sinopharm Chemical Reagent Co., Ltd.), potassium hydroxide (KOH, > 85%, Sinopharm Chemical Reagent Co., Ltd.), acetonitrile (CH_3CN, 99%, Sinopharm Chemical Reagent Co., Ltd.) CO_2 gas (> 99.999%, Guangming, Dalian, China). Ultrapure water is obtained by the ELGA filtering system.

In a typical procedure[1] for the synthesis of Rh:Cu_2O, y mL Na_3RhCl_6 aqueous solution (1.3 μM) (y = 0.6, 1.2, 3.6 for different 0.005%, 0.01% and 0. 03% molar ratio of Rh:Cu), 4 mL oleic acid (OA) and 20 mL absolute ethanol were added successively into 40 mL $CuSO_4$ aqueous solution (0.025 M) under vigorous stirring. The solution was heated to 373 K and then 10 mL NaOH aqueous solution (0.8 M) was added. After stirring for 5 min, 30 mL D-(+)-glucose aqueous solution (0.63 M) was added. The resulting mixture was stirred at 373 K for additional 1 h and gradually turned into a brick-red color. The resulting precipitate was collected by centrifugation, decanted by repeated washing with distilled water and absolute ethanol, and finally dried in vacuum at room temperature (RT) overnight. The products of different Rh:Cu molar ratio is denoted as x%-Rh:Cu_2O (x = 0.005, 0.01, 0.03). The synthetic process of Rh:Cu_2O is

shown as follows:

$$Cu^{2+} + 2OH^- \rightarrow Cu(OH)_2 \downarrow \quad (1)$$

$$2Cu(OH)_2 + CH_2OH(CHOH)_4CHO \rightarrow CH_2OH(CHOH)_4COOH + Cu_2O \downarrow + 2H_2O \quad (2)$$

$$3Cu_2O + 2Rh^{3+} + 6OH^- \rightarrow 2Rh + 6CuO + 3H_2O \quad (3)$$

$$2CuO + CH_2OH(CHOH)_4CHO \rightarrow CH_2OH(CHOH)_4COOH + Cu_2O \quad (4)$$

Cu_2O was prepared in parallel to Rh:Cu_2O by the same method without addition of Na_3RhCl_6. Post-Rh-Cu_2O was prepared in parallel to Rh:Cu_2O except that same amount of Na_3RhCl_6 aqueous solution was added after Cu_2O growth and then kept heating for another 20 min before centrifugation.

2. Preparation of electrodes

The electrode for tests in an H-type cell was prepared by drop casting the catalyst ink on a carbon paper (Toray, H060). The ink was a mixture of 2 mg catalyst, 60 μL water, 90 μL ethanol and 50 μL Nafion solution (1 wt.% in ethanol), ultrasonically dispersed for 30 min. The mass loading of catalyst was 1 mg cm^{-2}.

The electrode for tests in a flow cell was prepared by spraying the catalyst ink onto a commercial gas diffusion electrode (Freudenberg H14C9). Typically, the catalyst ink was composed of catalyst, and Nafion ionomer dispersed in i-propanol by sonicating for 30 min. The total mass loading of catalyst was around 1.0 mg cm^{-2}.

3. Materials characterizations

Samples were characterized by X-ray diffraction (XRD) on a Rigaku D/Max-2500/PC powder diffractometer using Cu Kα radiation (40 kV × 200 mA). The morphologies of prepared samples were detected with scanning electron microscopy (SEM, Hitachi Quanta 200F), field emission scanning electron microscopy (FESEM, Hitachi JSM-7900F) equipped with an energy dispersive X-ray spectrometer (EDS), and high-resolution transmission electron microscopy (HRTEM, JEOL JEM-2000EX). The high angle annular dark field scanning transmission electron microscopy (HAADF-STEM) images were taken on a probe-corrected JEM-ARM200F electron microscope

equipped with an energy dispersive X-ray spectrometer (EDS). X-ray photoelectron spectroscopy (XPS) measurements were performed using a Thermofisher ESCALAB 250Xi spectrometer with Monochromated Al Kα excitation (1486.6 eV, 15 kV, 10.8 mA). For the elemental ICP measurements (ICP-OES, PerkinElmer ICPS-8100), samples were dissolved by 2 M HNO_3. Temperature-programmed desorption measurements with a mass detector (TPD-MS) were conducted using a Micromeritics AutoChem 2920 system with a TCD detector and coupling to an OmniStar 300 mass spectrometer.

4. Electrochemical measurements

The linear sweep scans were collected in a standard three-electrode system equipped with the CHI 660e electrochemical workstation.

For tests in the H-type cell, an Ag/AgCl reference electrode, a Pt counter electrode and a Nafion-117 membrane were used. Otherwise mentioned, all potentials in the H-type cell were used without iR compensation and were converted with respect to reversible hydrogen electrode (RHE) scale by equation: $E_{RHE} = E_{Ag/AgCl} + 0.1976\ V + 0.059 \times pH$. The pH values of 0.5 M $KHCO_3$ saturated with Ar and CO_2 were 8.3 and 7.5, respectively. The selectivity and reaction rate of CO_2RR were evaluated by controlled-potential electrolysis. Electrolytes were pre-saturated and bubbled with CO_2 during measurements.

For the tests in the flow cell, Ag/AgCl with electrolytic bridge was used as reference electrode, and Ni foil was used as count electrode. All potentials in the flow cell were converted to RHE and corrected for iR drop: $E_{RHE} = E_{Ag/AgCl} + 0.1976\ V + 0.059 \times pH - iR \times 80\%$. The gas diffusion electrode with catalysts, anion exchange membrane (fumasep FAA-3-PK-130), and nickel anode were combined together by using PEEK spacers so that liquid electrolytes could be introduced into the cathodic and anodic chambers. A home-made flow cell is designed according to the literatures.[2, 3] The anodic and cathodic chambers are filled with flowing electrolyte and separated with the membrane. The gas chamber is filled with CO_2. The dimension of the flow channels was 2 cm × 0.5 cm × 0.15 cm. The CO_2 flow rate was 20 mL min^{-1}, controlled by a mass flow controller. 1 M KOH was circulated with peristaltic pump and the flow

rate of the electrolytes at 3.036 mL min^{-1}. In addition, the cathodic electrolyte was bubbled with Ar during measurements.

The electrochemically active surface area (ECSA) was calculated from the double-layer capacitance (C_{dl}) in the none-Faradic region by conducting cyclic voltammetry tests under different scan rates. As Cu_2O can easily undergo redox reactions and there is water splitting reaction in 1 M KOH, it is difficult to find the none-Faradic region. So, the cyclic voltammetry curves were measured in CH_3CN solution (0.1M $BminPF_6$) saturated with Ar within a none-faradaic potential region (−0.21 V to −0.11 V *vs.* RHE for Rh:Cu_2O and Cu_2O, 0.1 V to 0.2 V *vs.* RHE for glass carbon electrode). Ten cycles were recorded at each scan rate and the current values were taken during the last cathodic scan at 0 V. The linear slopes k can be obtained from $\Delta J/2 = (J_a - J_c)/2$ against scan rates, and $k = C_{dl}$. To note that, the relative electrochemical surface area estimated from the double layer capacity current included the contribution of the exposed C substrate.

5. Product analysis

Gas products (H_2, CO, CH_4 and C_2H_4) were quantified by an online gas chromatograph (GC, Agilent 7890A, Ar carrier and Agilent Parapok Q packed column) equipped with TCD (for H_2 detection), FID detectors and a methanizer (for CO and CH_x detection). The gas flowed through the cell at a constant flow and was vented into the sampling loop of the GC. Liquid products were analyzed by a Bruker AVANCE III 400 MHz nuclear magnetic resonance (NMR) spectrometer. A mixture of liquid electrolyte, DMSO (internal standard) and D_2O was used for NMR measurements. The one dimensional ^1H spectrum was measured with water suppression using a presaturation method.

6. Computational details

All calculations were carried out in Vienna Ab-initio Simulation Package (VASP) based on spin-polarized density functional theory (DFT).[4, 5] The exchange–correlation energy was expressed by the generalized gradient approximation with Perdew–Burke–Ernzerhof (GGA-PBE) functional,[6] and the projector augmented wave (PAW) pseudopotential was used to represent core electrons effects.[7, 8] Cu(100) was modeled

with a 5×5×4 supercell slab in a 15 Å vacuum. Due to the vacuum, dipole corrections were implemented. To resemble the real bulk material and the surface, respectively, two bottom layers were fixed in their positions while the two top layers were free to move due to interaction with the adsorbates. The cutoff energy was set to be 500 eV and Gaussian electron smearing method with σ = 0.05 eV were used. The empirical dispersion correction (DFT-D3) method was applied to describe the long-range van der Waals (vdW) interactions in layered materials.[9] The convergence tolerance for residual force and energy on each atom during structure relaxation was set to 0.02 eV/Å and 10^{-5} eV, respectively. The Monkhorst-Pack k-point mesh was set to be 3×3×1.

The CO adsorption energy was calculated as:

$E_{ads} = E_{*CO} - (E_{*} + E_{CO})$

Where, E_{*CO} was the electronic structure energy of the adsorbed CO on the catalyst, E_{*} was the energy of the slab, and E_{CO} was the CO energy in gas phase without the catalyst.

The CO-CO coupling energy barrier was calculated according to the following reaction and the corresponding reaction free energy:

*OCCO =*CO +*CO

$E_{\text{C-C coupling barrier}} = E_{*OCCO} - (E_{*CO} + E_{*CO})$

The reaction free energies were approximated as $\Delta G = \Delta E + \Delta ZPE - T\Delta S$, where ΔE was the DFT calculated reaction energy, ΔZPE and $T\Delta S$ were the zero-point energy correction and the entropy change at room temperature (298.15 K). The computational hydrogen electrode was used to model proton-electron pairs.[10]

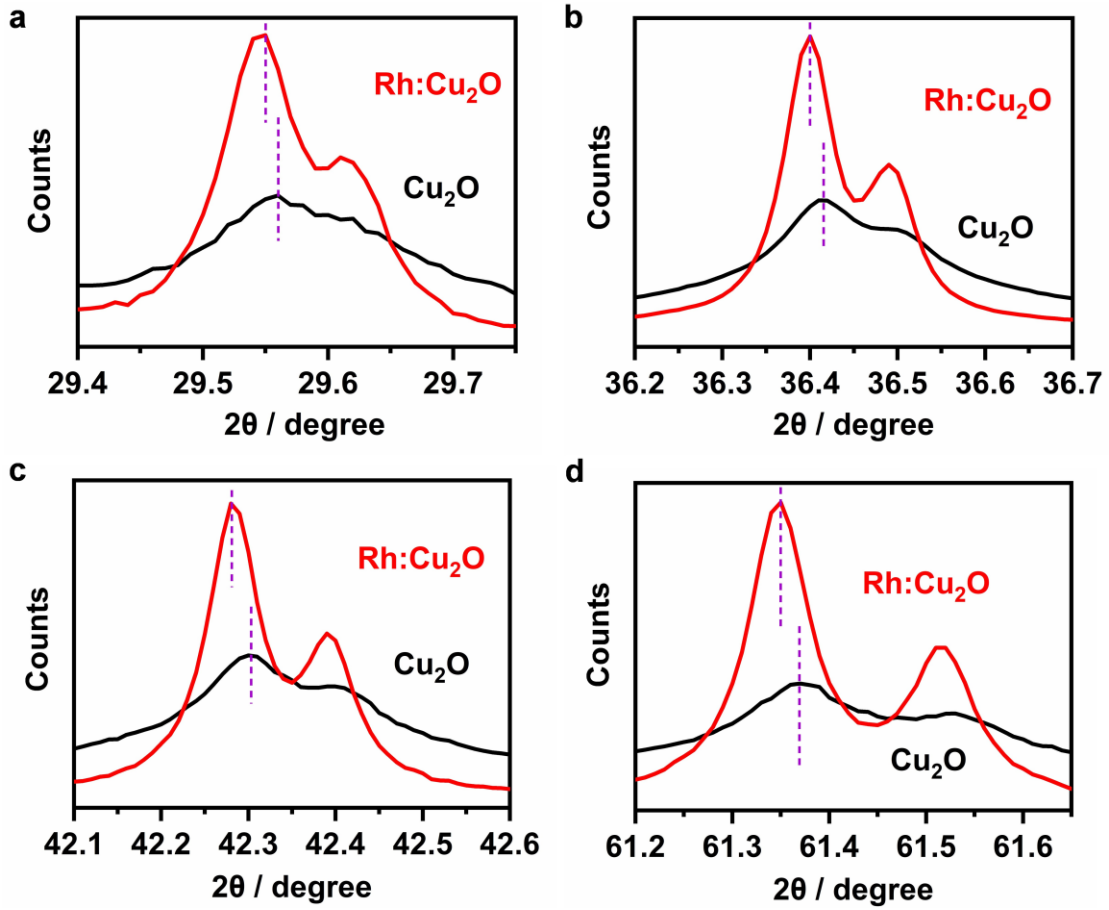

Figure S1. The fined XRD patterns for Rh:Cu_2O and Cu_2O powders supported on carbon paper with no binders. The red and black lines represent Rh:Cu_2O and Cu_2O respectively.

Each characteristic peak of Cu_2O slightly shifts to smaller angle for around 0.02°, which illustrates the doping of Rh into Cu_2O.

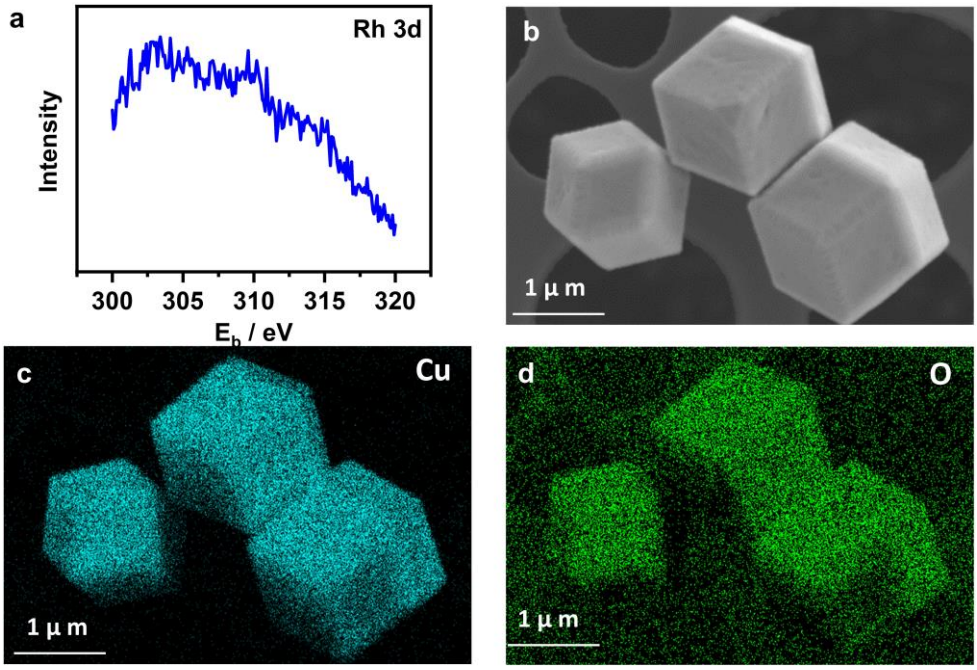

Figure S2. The (a) Rh 3d XPS spectra of Rh:Cu_2O. All signals were calibrated by C 1s (284.6 eV). (b-d) The element mapping results of 0.1%-Rh:Cu_2O tested on FESEM.

Table S1. Ratio of Rh to Cu in different samples determined by the ICP measurements.

Samples	Molar ratio n(Rh)/n(Cu)	Mass ratio m(Rh)/m(Cu)
Rh:Cu_2O	0.004%	0.006%
post-Rh-Cu_2O	0.0005%	0.0007%

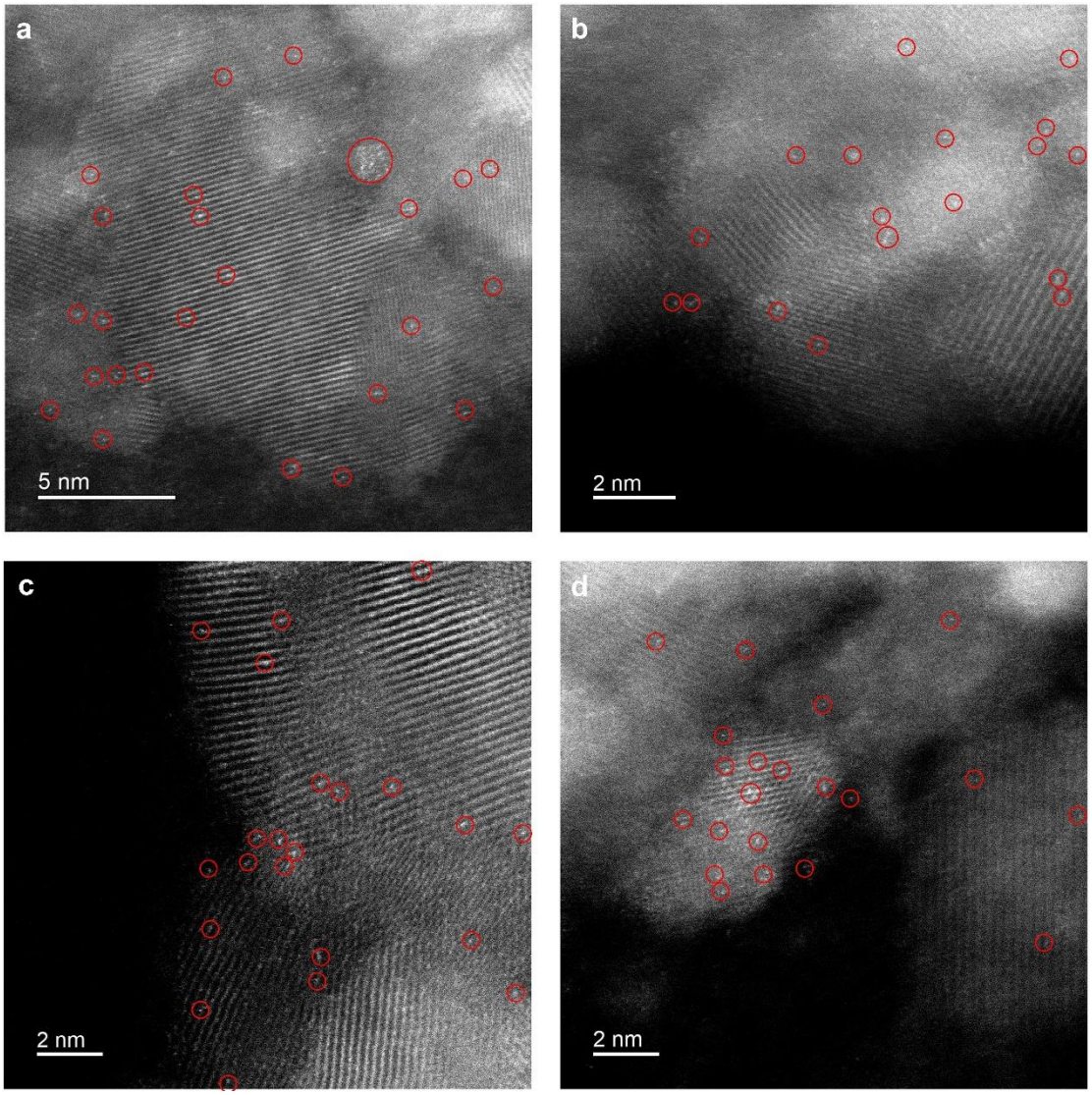

Figure S3. The HADDF-STEM images of Rh:Cu_2O. Atomically dispersed Rh atoms were marked with red circles.

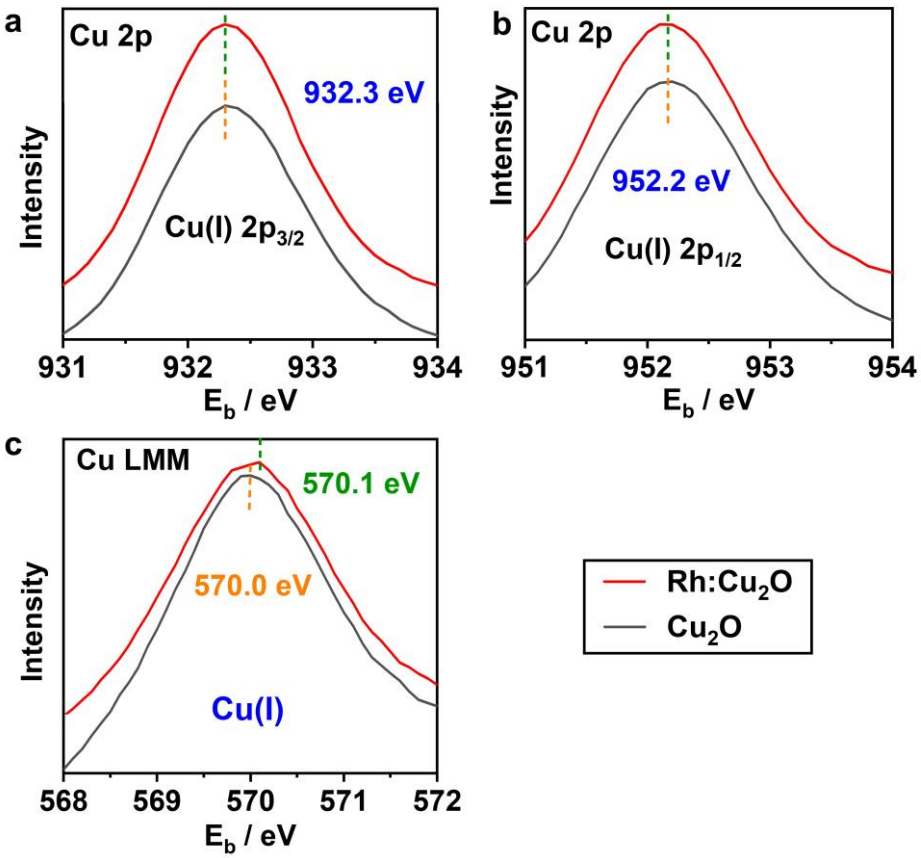

Figure S4. The local enlarged XPS and Auger spectra for Rh:Cu_2O and Cu_2O.

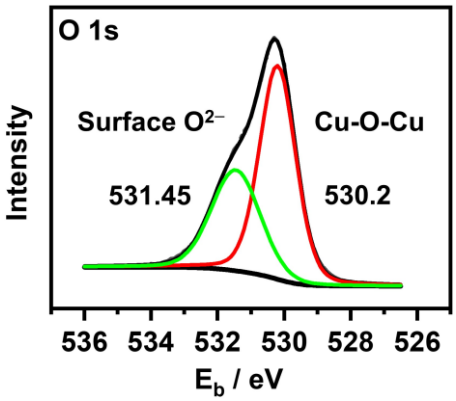

Figure S5. High resolution O 1s XPS spectra of Rh:Cu_2O catalysts. All signals were calibrated by C 1s (284.6 eV).

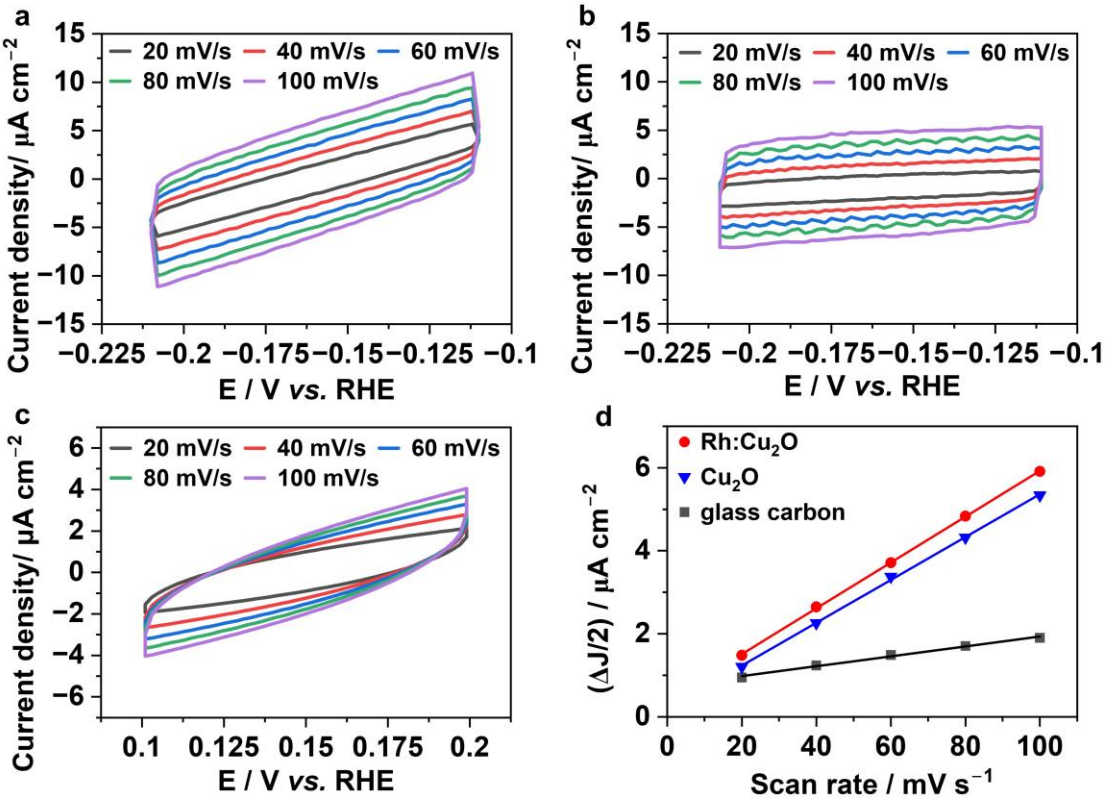

Figure S6. (a-c) The CV curves of Rh:Cu_2O, Cu_2O and glass carbon in CH_3CN solution (0.1M $BminPF_6$) saturated with Ar. (d) Half of the capacitive current density of different catalysts in CH_3CN solution (0.1M $BminPF_6$) as a function of scan rate over a non-faradic potential range.

Based on the data in **Figure S6**, the calculated double-layer capacitances of Rh:Cu_2O, Cu_2O and glass carbon are 55.2, 51.6 and 11.9 μF cm^{-2}, respectively. Supposing the geometric area of the glass carbon electrode is 1 cm^2, the relative electrochemical active surface area of Rh:Cu_2O and Cu_2O is 4.63 and 4.33 cm^2, respectively.

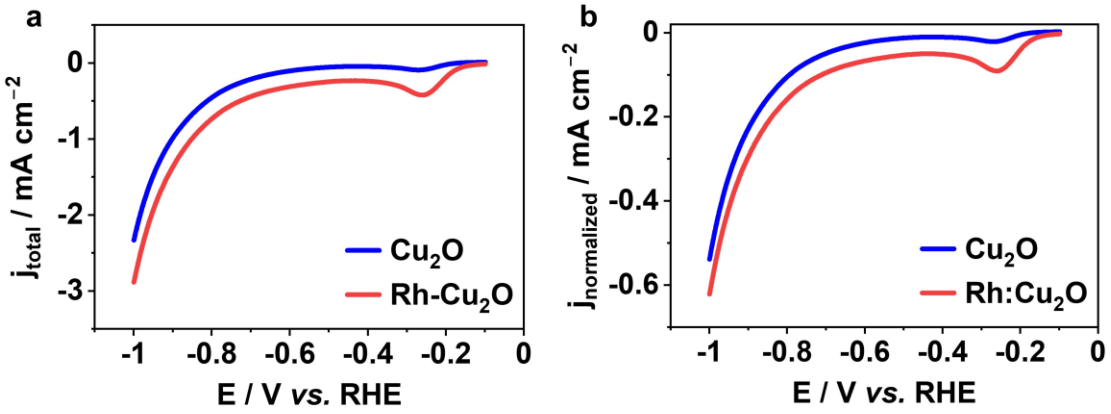

Figure S7. (a) The LSV scans of Rh:Cu_2O and Cu_2O in an H-type cell with 0.5 M $KHCO_3$ saturated with CO_2. (b) The ECSA-normalized LSV curves of Rh:Cu_2O and Cu_2O in an H-type cell with 0.5 M $KHCO_3$ saturated with CO_2.

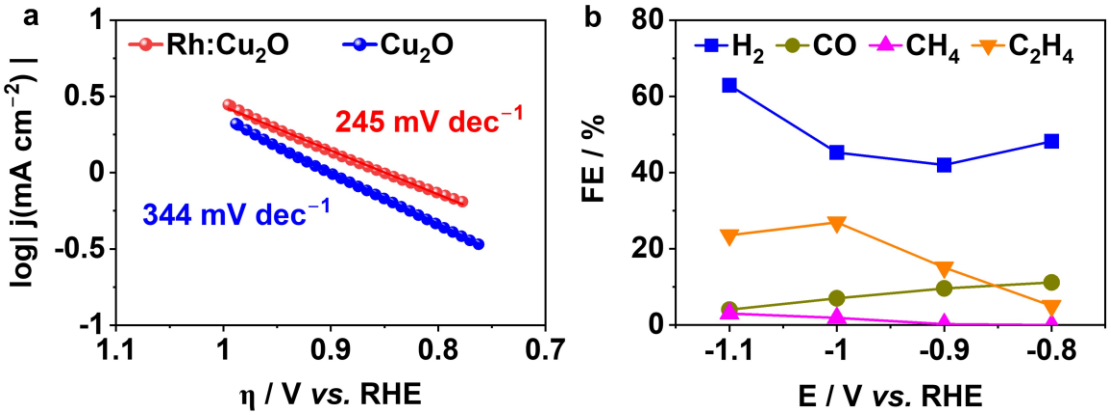

Figure S8. (a) The Tafel plots of Rh:Cu_2O and Cu_2O, and (b) FEs of gas products of CO_2RR with Rh:Cu_2O at different potentials. Condition: in an H-type cell with 0.5 M $KHCO_3$ saturated with CO_2.

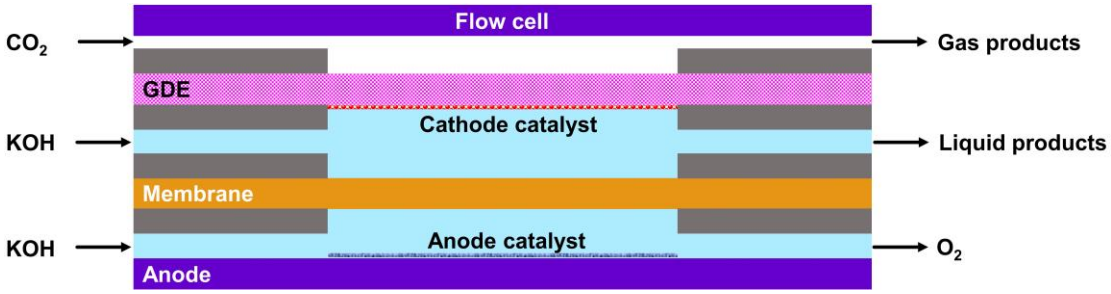

Figure S9. A schematic diagram of the flow cell.

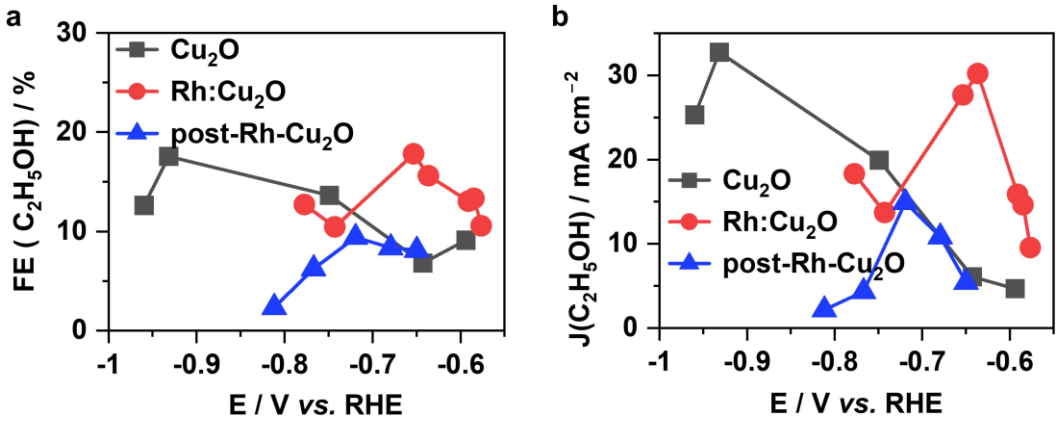

Figure S10. (a) FE(C_2H_5OH) and (b) J(C_2H_5OH) on Cu_2O, Rh:Cu_2O and post-Rh-Cu_2O at different potentials in a flow cell.

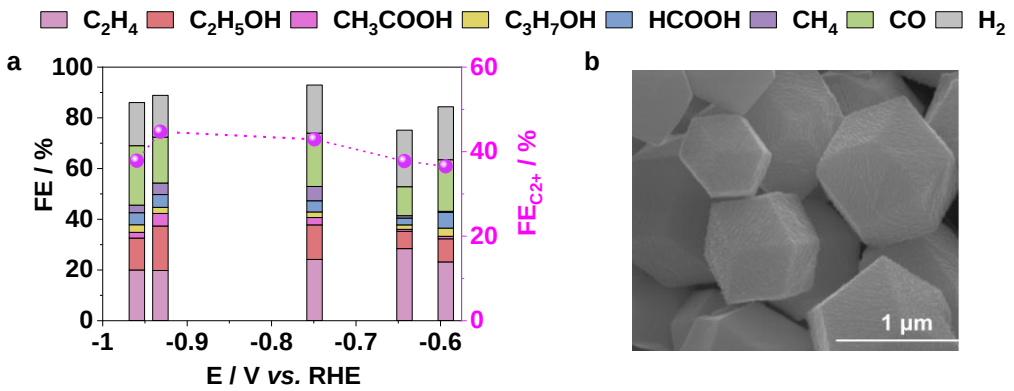

Figure S11. (a) FEs of various products on post-Rh-Cu_2O at different potentials in a flow cell. (b) SEM images of post-Rh-Cu_2O.

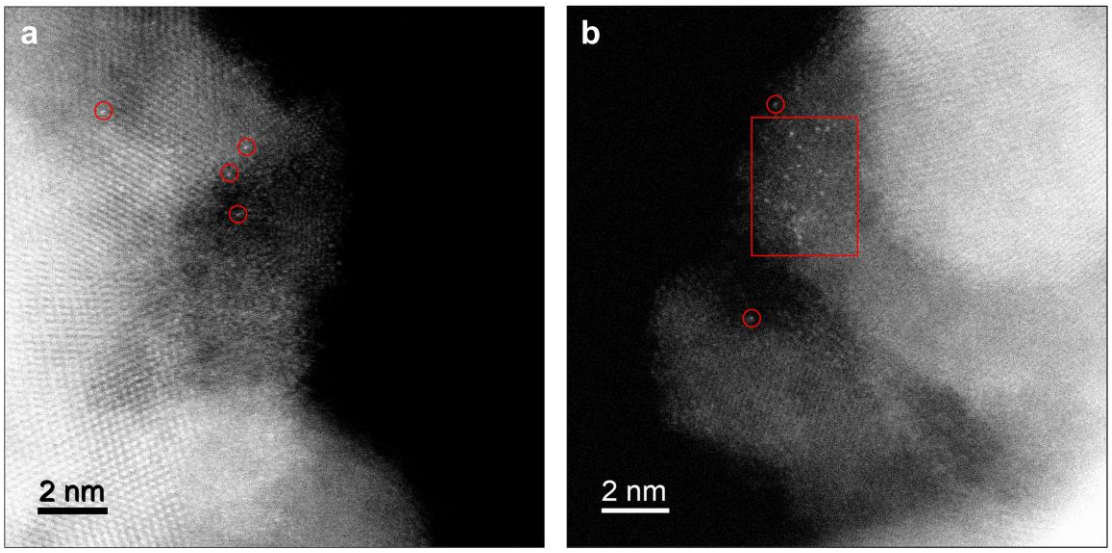

Figure S12. HAADF-STEM images of Rh in post-Rh-Cu_2O.

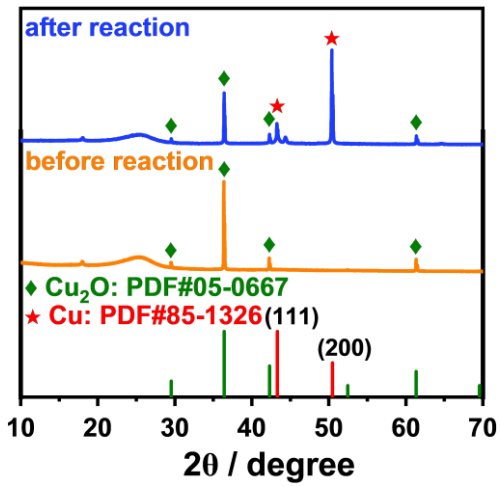

Figure S13. XRD patterns of Rh:Cu_2O before and after CO_2RR reduction.

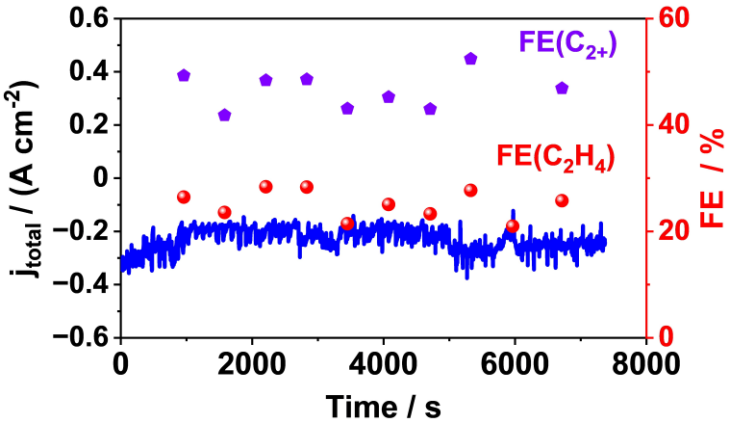

Figure S14. The durability test of Rh:Cu_2O at around −0.68 V assessed in the flow cell.

It shows that the FE(C_{2+}) and FE(C_2H_4) maintain at around 46.5% and 25.1% respectively during 2 h.

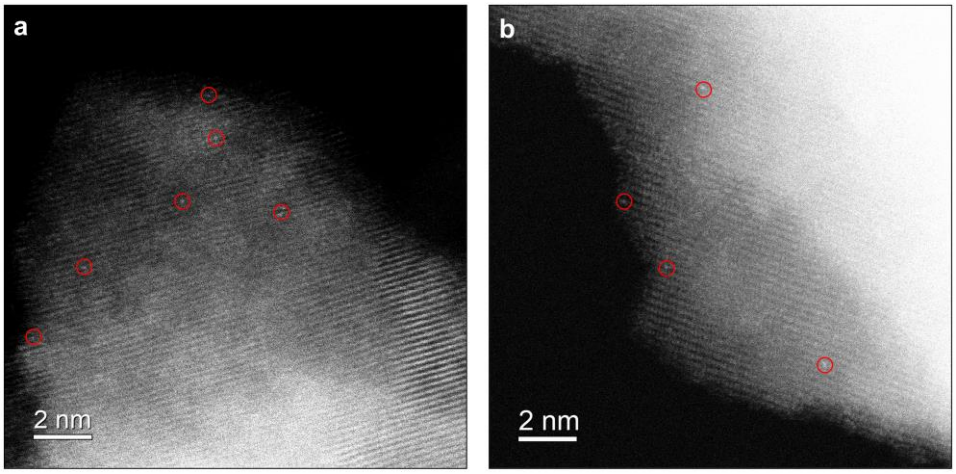

Figure S15. HAADF-STEM images of Rh:Cu_2O after electrolysis.

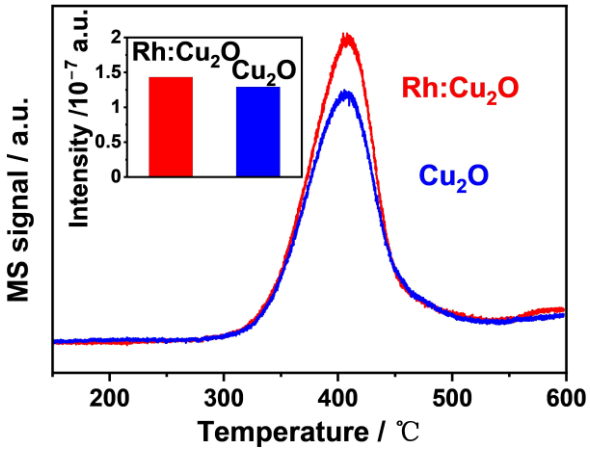

Figure S16. CO_2 TPD-MS spectra of Rh:Cu_2O and Cu_2O. To clearly identify the desorbed CO_2 signal, the mass-to-charge (m/z) ratio was set at 44.

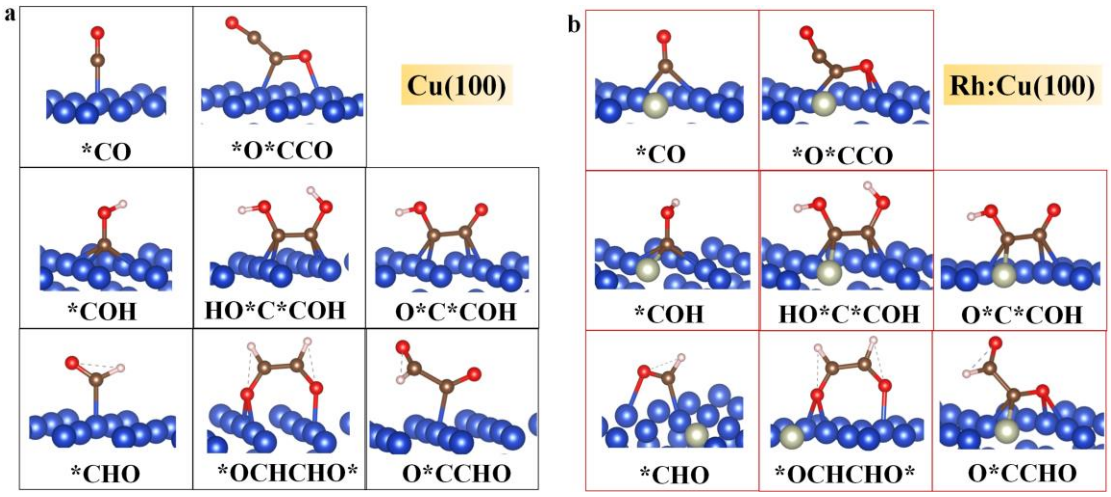

Figure S17. Optimized structures of main adsorption intermediates. The structures of intermediates during CO_2RR to ethylene and ethanol on (a) Cu(100) surfaces and (b) Rh:Cu(100) surfaces. The blue, white, brown, red and pink balls represented Cu, Rh, C, O and H, respectively.

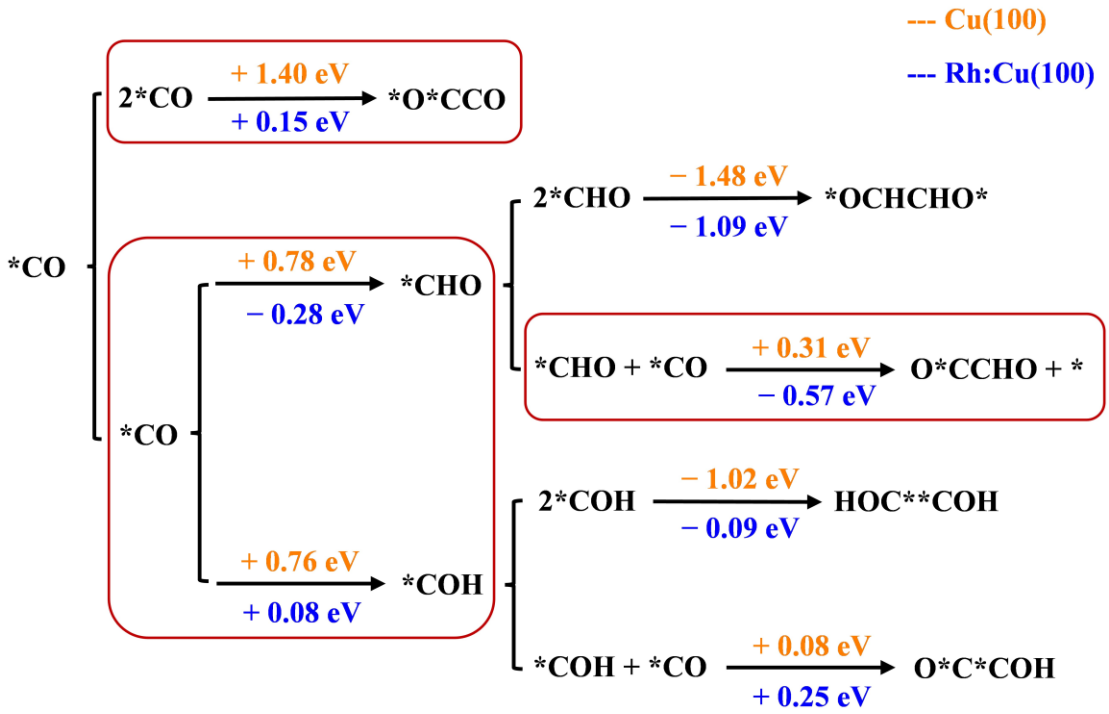

Figure S18. The changes of Gibbs free energy (ΔG) of different C−C coupling pathways. The orange and blue numbers represented the ΔG on Cu(100) and Rh:Cu(100) surfaces, respectively.

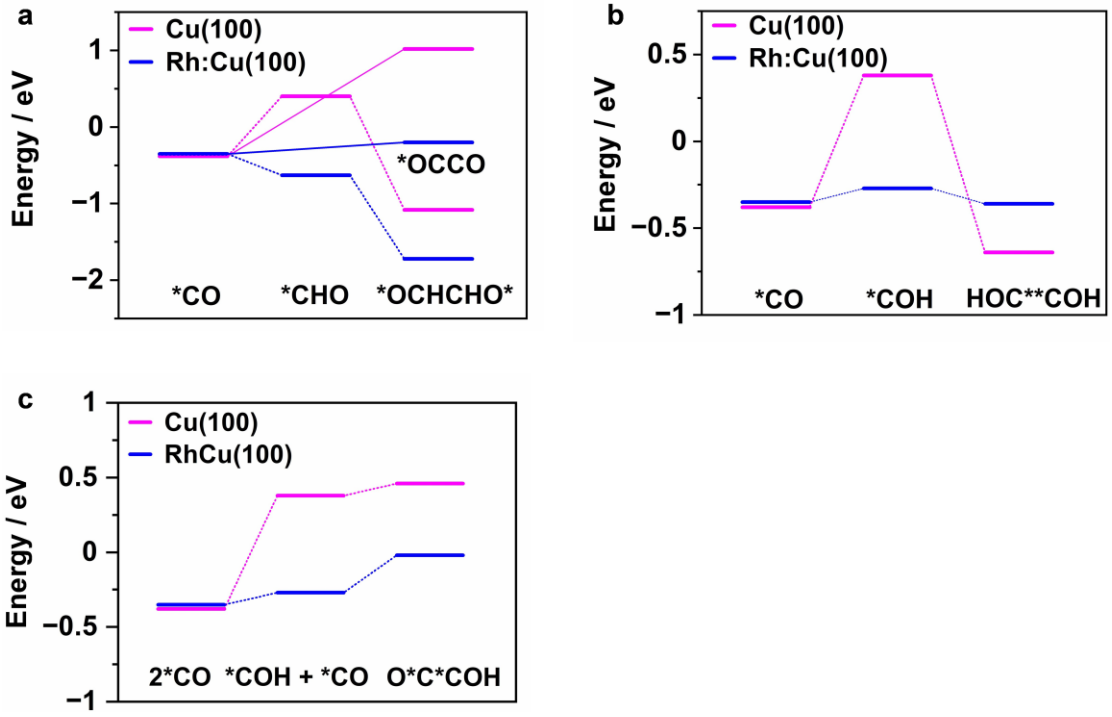

Figure S19. The changes of Gibbs free energy (ΔG) of possible different C−C coupling pathways.

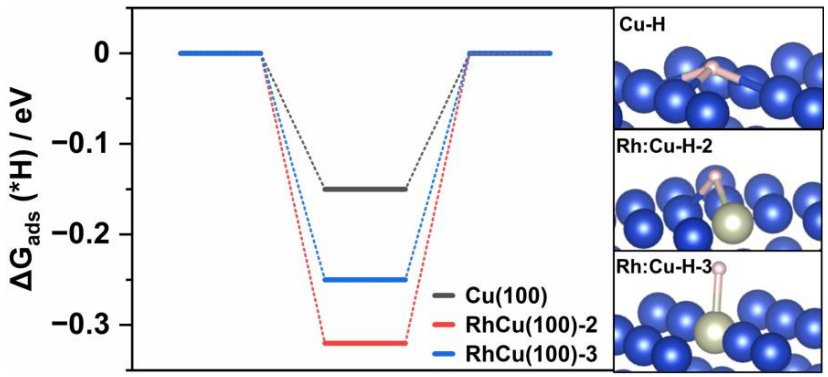

Figure S20. The changes of Gibbs free energy (ΔG_{ads}(*H)) of hydrogen atom adsorption on Rh:Cu(100) and Cu(100) surface with different configurations.

It shows that the energy barrier of hydrogen atom adsorption (*H) on Cu sites adjacent to Rh atoms is much lower (−0.32 eV) that on pristine Cu sites (−0.15 eV).

References

1.Z. Zhang, S. S. Wang, R. Song, T. Cao, L. Luo, X. Chen, Y. Gao, J. Lu, W. X. Li, W. Huang, *Nat. Commun.*, 2017, **8**, 488.

2.S. Ma, M. Sadakiyo, R. Luo, M. Heima, M. Yamauchi, P. J. A. Kenis, *Journal of Power Sources*, 2016, **301**, 219-228.

3.C. T. Dinh, T. Burdyny, M. G. Kibria, A. Seifitokaldani, C. M. Gabardo, F. P. G. d. Arquer, A. Kiani, J. P. Edwards, P. D. Luna, O. S. Bushuyev, C. Zou, R. Quintero-Bermudez, Y. Pang, D. Sinton, E. H. Sargent, *Science*, 2018.

4.G. Kresse, J. Furthmüller, *Comput. Mater. Sci.*, 1996, **6**, 15-50.

5.G. Kresse, J. Furthmüller, *Phys. Rev. B*, 1996, **54**, 11169-11186.

6.J. P. Perdew, K. Burke, M. Ernzerhof, *Phys. Rev. Lett.*, 1996, **77**, 3865-3868.

7.P. E. Blöchl, *Phys. Rev. B*, 1994, **50**, 17953-17979.

8.G. Kresse, D. Joubert, *Phys. Rev. B*, 1999, **59**, 1758-1775.

9.S. Grimme, J. Antony, S. Ehrlich, H. Krieg, *J. Chem. Phys.*, 2010, **132**, 154104.

10.J. K. Nørskov, J. Rossmeisl, A. Logadottir, L. Lindqvist, J. R. Kitchin, T. Bligaard, H. Jónsson, *J. Phys. Chem. B*, 2004, **108**, 17886-17892.